ON THE PLASTIC STRAIN ACCUMULATION IN NOTCHED BARS DURING HIGH TEMPERATURE CREEP DWELL

Daniele Barbera

School of Engineering, System and Power Division
University of Glasgow
Glasgow, UK

Haofeng Chen*

Department of Mechanical & Aerospace Engineering
University of Strathclyde
Glasgow, UK

ABSTRACT

Structural integrity plays an important role in any industrial activity, due to its capability of assessing complex systems against sudden and unpredicted failures. The work here presented investigates an unexpected new mechanism occurring in structures subjected to monotonic and cyclic loading at high temperature creep condition. An unexpected accumulation of plastic strain is observed to occur, within the high-temperature creep dwell. This phenomenon has been observed during several full inelastic finite element analyses. In order to understand which parameters make possible such behaviour, an extensive numerical study has been undertaken on two different notched bars. The notched bar has been selected due to its capability of representing a multiaxial stress state, which is a practical situation in real components. Two numerical examples consisting of an axisymmetric v-notch bar and a semi-circular notched bar are considered, in order to investigate different notches severity. Two material models have been considered for the plastic response, which is modelled by both Elastic-Perfectly Plastic and Armstrong-Frederick kinematic hardening material models. The high-temperature creep behaviour is introduced using the time hardening law. To study the problem several results are presented, as the effect of the material model on the plastic strain accumulation, the effect of the notch severity and the mesh element type and sensitivity. All the findings further confirm that the phenomenon observed is not an artefact but a real mechanism, which needs to be considered when assessing off-design condition. Moreover, it might be extremely dangerous if the cyclic loading condition occurs at such a high loading level.

Keywords: Plasticity, Creep, Structural Integrity.

1. INTRODUCTION

Mechanical structures are designed to withstand defined loading conditions, which includes monotonic and cyclic thermal and mechanical loads. Different international design codes and assessment procedures are currently adopted, like the UK's R5 procedure [1] and the ASME NH [2]. For each code, it is important that the structure does not fail during operative life, even in the case of severe accidents or malfunctions. This important issue can be tackled by adopting a fail-safe design and making sure that the safety margins are correctly estimated. Due to the severe consequences of chemical and radiation release on society, these industrial structures have rigid requirements in terms of safety. Several aspects need to be considered and one of these is the accurate prediction of structural response of component subjected to an extreme load. The estimate of the deformations and times to failure in such an extreme scenario will contribute to improving the resilience of the design.

In standard design codes and assessment procedures like the ASME NH and the UK's R5, the plastic deformation due to monotonic loading is one of the very first analysis to be performed. More specifically for the R5, when a structure is under creep condition and subjected to a monotonic mechanical load the rupture stress is analytically estimated by using elastic solution and the following relationship:

$$\sigma_{ref}^{R} = \left\{1 + 0.13\left[\chi - 1\right]\right\}\sigma_{ref} \tag{1}$$

* Corresponding author (haofeng.chen@strath.ac.uk)

Where σ_{ref} is the reference stress and it is calculated using different formulations depending on the load condition. For an isothermal and homogenous structure it is equal to $\sigma_{ref} = P\sigma_y / P_U$, where P is the primary load, σ_y is the yield stress of the material and P_U is the plastic collapse load. χ is the stress concentration factor, and it is used to adjust the reference stress for local strain concentration. For an isothermal and homogenous structure, it is obtained as the ratio between the maximum elastic equivalent stress in the structure and the maximum reference load calculated. In the literature, extensive work is available for modelling the damage induced by high-temperature creep under monotonic load, especially in notched bars [3-7] using continuum damage mechanics.

As it is well-known creep failure is the result of a progressive inelastic deformation, which occurs when a material is subjected to a mechanical load, at high temperature. In the common practice creep and plastic damage are estimated in a separated way. Creep damage growth and propagation across the material is related to the growth and coalescence of voids in the microstructure of the material. This is a general description that is behind a very complex process, which can be expressed as the results of three different behaviours. The first one regards the cross-section reduction due to the material deformation. Such a reduction of area is mandatory to respect the volume constancy. The second regards the material behaviour at high temperature that can exhibit particular phenomena like recrystallization and the development of precipitates. The third one is the development of the defects. The introduction of these defects causes a local increase in the stress and the local intergranular cracking. To numerically model the creep rupture several continuum damage mechanics models have been proposed and validated. Two of the most used are the Kachanov-Rabotnov model [8, 9] and the Liu Murakami [10], which introduce a scalar damage parameter. These and other models subsequently developed share the same idea that a creep damage parameter is used to regulate the stress and strain relationship. At the start of the creep dwell, no damage is present within the volume of material considered, or it is too small to affect the stress-strain response. However, when sufficient time has passed the damage will initiate and grows. The increase in the damage rate depends on the material properties and load conditions. A progressive smaller volume V of the body will be capable of bearing the applied load. While the failure front unifies and the damage propagates across the thickness of the component, the loading bearing capability is related to the redistribution of the stresses to the undamaged area. However, complete failure occurs when the undamaged volume reaches a limit beyond which it cannot bear the applied load. This process can be described by an accurate mathematical representation of the creep strain rate and damage rate. For a uniaxial creep problem the creep strain rate and the damage rate has been defined by the Kachanov-Rabotnov model as follow:

$$\dot{\varepsilon}_{ij}^{c} = \frac{3}{2} A \left(\frac{\bar{\sigma}}{1-\omega} \right) t^{m} \left(\frac{S_{ij}}{\bar{\sigma}} \right)$$
$$\dot{\omega} = B \frac{\sigma_r^{\chi}}{(1-\omega)} \tag{2}$$

Where $\bar{\sigma}$ is the von Mises stress, S_{ij} is the deviatoric stress component and σ_r is the rupture stress and t is the time. All the other multipliers or exponents are material parameters, which require being calculated by tensile creep tests. However, this constitutive damage model is not complete because it requires the definition of the rupture stress for the damage rate calculation. The rupture stress is calculated considering the effect of both principal stress and equivalent stress, using the following formulation:

$$\sigma_r = \alpha\sigma_1 + (1-\alpha)\bar{\sigma} \tag{3}$$

α is the multiaxial parameter, and it describes the effect of principal σ_1 and von Mises stress $\bar{\sigma}$ on the failure mechanism. To obtain such a creep parameter, a tensile test needs to be done on a notched bar specimen. When the rupture life is known at different applied stresses, FE-analyses are performed varying α and an optimum value is identified. However, this procedure is tedious and requires many experimental and numerical tests. Furthermore, it has been demonstrated that the rupture life is significantly affected by the predicted parameters [11]. Despite its simplicity, the Kachanov creep damage model has a clear weakness in its mathematical formulation. When the damage parameter approaches to the unity, the creep strain rate and damage rate tend to diverge to infinite. This problem has been resolved by the model presented by Liu-Murakami and then successfully applied to several engineering problems [12].

Several local creep damage models have been developed, with even more damage parameters. However these stress based damage models have two major drawbacks, the first one regards their applicability. The material parameters need to be calibrated using precise testing conditions, such as load level and temperature. In some cases such as the Dyson model, this procedure can be very complex [7, 13]. This makes it very challenging to apply these models for standard design procedure, where versatility and flexibility are preferred. In addition, in these works, the contribution of plasticity to the overall failure mechanism is considered negligible compared to creep. In a similar way, a large number of works have been done to estimate the creep-fatigue life of components using numerical methods based on complex constitutive models [6, 14-16] or by approximated methods [17-20]. However, for all the cases introduced the loading conditions have been well below certain levels, and not even close to the plastic limit of the structure.

The study proposed is relevant for component's safety when non-conventional loading conditions occur, leading to the detrimental accumulation of inelastic strain, with emphasis on high-temperature conditions. A new important but usually ignored failure mechanism associated with the increase of the plastic strain during the creep dwell is discussed. It has been identified and investigated by numerical finite element analyses on notched bars, subjected to high mechanical load level and high-temperature. Notched bars are considered due to their capability of representing more realistically the multiaxial stress state in real components. Two material models for cyclic plastic response have been considered, the Elastic Perfect Plastic (EPP) material model widely adopted for structure assessment and the more refined combined hardening model. The monotonic load has been considered as well, and the plastic behaviour has been modelled using the stress-strain curve. In order to prove that this mechanism is not a numerical artefact, both the element type and mesh sensitivity have been investigated. The aim of this paper is to identify, discuss and explain this new failure mechanism

2. METHODS OF SOLUTION

2.1 Finite Element Models

The v-notched and the c-notched bar are both shown in Figure a-b and all the geometrical properties are reported as well. The mesh is refined in the notched area, and the entire model is composed of 1394 and 600 elements respectively. The semicircular notched bar is shown in Figure b, the radius is 9 mm and the throat depth is 4.5 mm. For both the numerical models a 2D axis-symmetric 8 node quadrilateral element with a reduced integration scheme is adopted. The v-notched bar has a Kt equal to 5, which will lead to an extremely high level of stress with a relatively small applied load, instead, the semicircular notched bar has a Kt equal to 1.4. The mechanical load is applied to the top of the bar and fully fixed boundary condition is applied on the bottom side. When a cyclic load is required the applied constant mechanical load is accurately scaled to reproduce the desired load cycle with an R= 0.

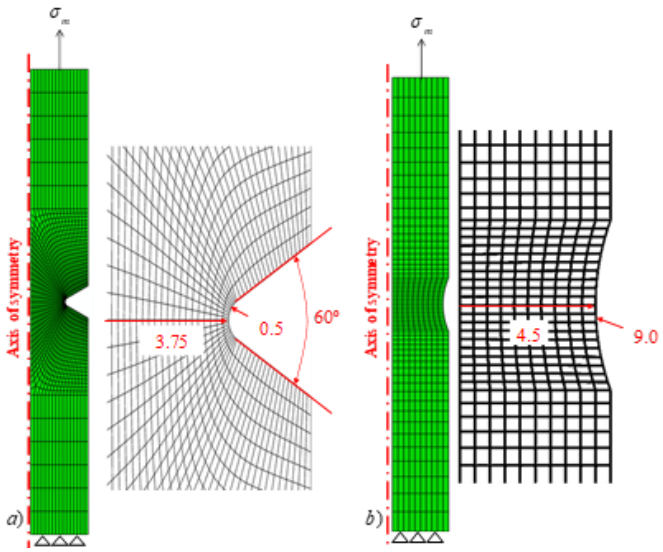

Figure 1 Finite element model and geometry properties for the a) v-notched bar and b) c-notched bar.

For both the monotonic and cyclic load case the Elastic Perfect Plastic (EPP) material model has been used to study the impact of the model accuracy on the mechanism by understanding its effect on the magnitude and structural integrity significance of the new failure mechanism.

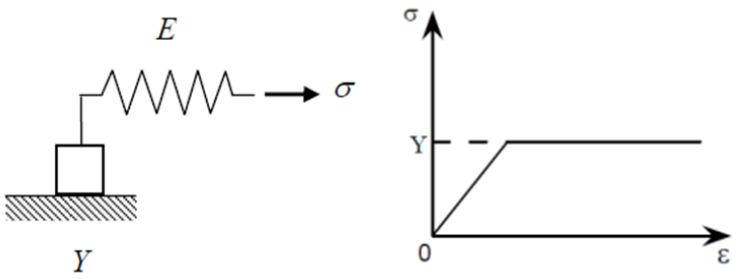

Figure 2 Schematic representation of the Elastic Perfect Plastic material model

The EPP material model has been used extensively in the past and represents one of the most used models for limit analysis of metallic structures, especially for initial design calculation. It can be represented by a very simple mass-spring model, shown in Figure 2. When the applied load σ is below the yield only elastic strain accumulates, and the mass is still fixed. However, when the applied load reaches the yield limit, plastic strain accumulates, and the mass starts to move. If the load is removed, the mass cannot return in its own original position, since there is no recall force, and this reflects the physical aspect of the plastic strain.

For the most complex cyclic load case, the EPP can be overly conservative and inaccurate, especially for material that exhibits complex responses under cyclic loads such as the Bauschinger effect or cyclic hardening/softening. The combined hardening model has been used to fully characterize the isotropic and kinematic hardening of the material.

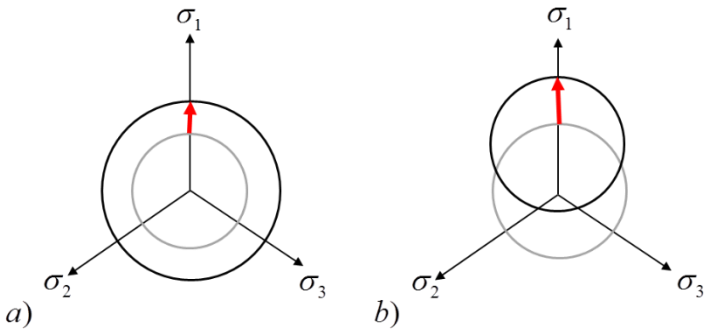

Figure 3 Schematic representation of a) isotropic and b) kinematic hardening

The isotropic hardening is used to describe the change of size of the yield surface to an associated accumulated plastic strain as shown in Figure 3a. This mechanism can be represented by a scalar function R, known as the drag stress introduced by [21]. The rate of change of this function is expressed by the following equation:

$$\begin{aligned} \dot{R} &= b\left(Q-R\right)\dot{\bar{\varepsilon}}_p \\ \dot{\bar{\varepsilon}}_p &= \sqrt{\frac{2}{3}\dot{\varepsilon}_p : \dot{\varepsilon}_p} \end{aligned} \tag{2}$$

Where $\dot{R}$ is the rate of change of the drag stress during the progressive hardening associated with an equivalent plastic strain rate $\dot{\bar{\varepsilon}}_p$ that can be defined by the plastic strain rate determined by the derivative of the plastic flow rule respect the stress tensor.

By integrating equation (2) with respect to the time the dimensional change of the updated yield surface σ_0 is given by:

$$\sigma_0 = \sigma_y + Q_\infty\left(1-e^{-b\varepsilon_p}\right) \tag{3}$$

Where σ_y is the initial yield stress, Q_∞ represents the asymptotic value of the yield stress, b defines the rate of change of the yield surface for an associated plastic strain ε_p. The yield criterion then can be expressed using the von Mises function:

$$f = \left|\sigma\right| - \sigma_0 = 0 \tag{4}$$

The isotropic hardening is capable of modelling the cyclic hardening by increasing the elastic limit $\left(\sigma_y + R\right)$ for an associated plastic strain. Furthermore, the isotropic softening can be modelled as well by considering a negative Q_∞, which tends to reduce the final saturated yield strength. Conversely, the kinematic hardening adopts a completely different concept to simulate the hardening/softening of materials. Rather than varying the yield surface dimension, the centre of the yield surface is rigidly translated within the stress plane as shown in Figure 3b. This modelling strategy is very important when tensile and compressive loads are present, and the Bauschinger effect needs to be considered. The yield surface drift is associated with a kinematic hardening parameter α, known as the back stress. The rate of change of the back stress is defined by the Armstrong-Frederick relationship as follow:

$$\dot{\alpha}_i = C_i \frac{1}{\sigma_0}\left(\sigma - \alpha\right)\dot{\varepsilon}_p - \gamma_i \alpha_i \dot{\varepsilon}_p$$
$$\dot{\varepsilon}_p = \frac{\partial f\left(|\sigma| - \alpha_i\right)}{\partial} \dot{\bar{\varepsilon}}_p \tag{5}$$

Where the first term presents the linear hardening, introduced earlier by Prager in 1949, and the second term expresses the non-linear behaviour introducing the recall coefficient γ_i, and $\dot{\varepsilon}_p$ is the plastic flow associated to the equivalent plastic strain rate $\dot{\bar{\varepsilon}}_p$. The non-linear recall effect is coupled with the plastic strain rate. C_i and γ_i are both material constants, and for each back stress, a couple of parameters need to be calculated. The overall back stress is calculated by the sum of each back stress component. The number of back stresses used affects directly the accuracy of the model adopted and three back stresses are normally used to fully describe the material behaviour for a wide strain range. However, in this work, single back stress is used due to the material constants provided by a third part.

The creep strain rate occurring during the constant tensile creep dwell is modelled using the Norton-Bailey law:

$$\dot{\varepsilon}_c = A \cdot \sigma^n \cdot t^m \tag{6}$$

Where A is the creep stress multiplier, n is the creep stress exponent and m is the creep time exponent. The material properties adopted for both notches and for monotonic, cyclic load and creep are shown in Table 1.

Table 1 Elasto-Plastic-Creep properties for the v and c notched bars for a generic structural steel.

Young's modulus [MPa]	Poisson's ratio	Yield Stress [MPa]	C_1	γ_1	Q_{inf}	b	A	n	m
148000	0.3	175	12374	150	99.8	37.7	4.08E-12	3.395	-0.535

3. RESULTS AND DISCUSSION

3.1 V-Notched and C-Notched Bar: Monotonic Load

In this subsection, the results for both the notched bars analysed using the EPP and isotropic strain hardening model are reported for different load cases. The effect of the load level is investigated by performing 3 analyses at 45, 60 and 90 MPa for the v-notched bar. The stress along the notch throat when using the EPP model are reported in Figure 4a, b and c respectively.

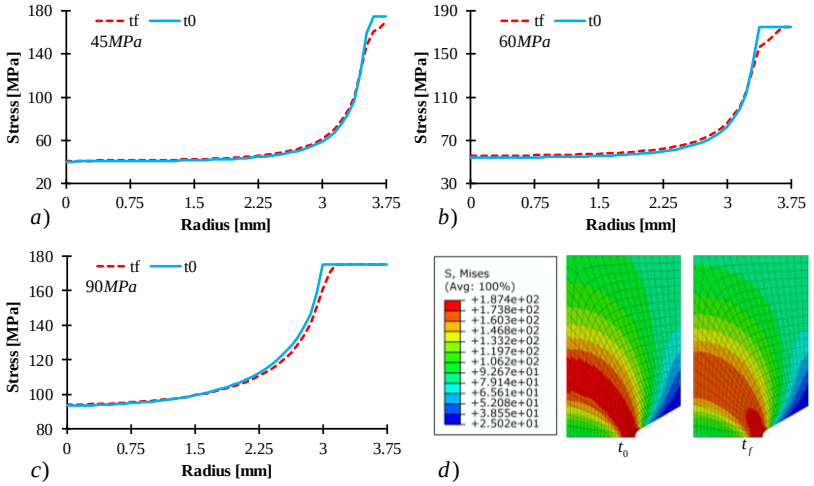

Figure 4 von Mises equivalent stress evolution along the notched bar throat for a) 45 MPa ,b) 60 MPa and c) 90 MPa, d) von Mises equivalent stress contours for the 90 MPa load case using the EPP model and a creep dwell of 1 hour.

In Figure 4a, the von Mises stress at the start of the dwell (t_0) and at its end (t_f) is shown. At the start of the creep dwell only the most exterior area of the notch is at the yield. When the creep dwell starts, stress relaxation occurs and rapidly a stress redistribution takes place and, no increase of the plastic strain is observed. However, by increasing the load up to 60 MPa the plastic strain accumulation starts during the creep dwell. At the end of the hold period, as shown in Figure 4b, the stress is only partially relaxed and a small region still at the yield but with a stress redistribution causing a localised accumulation of plastic strain. For the 90 MPa load case, the yielded area is larger than the 60 MPa case (Figure 4c). The corresponding von Mises stress contours at the start and end of the creep dwell are shown in Figure 4d. At the start of the creep dwell a larger area of the notch is yielded, but while stress redistributes during the creep dwell, most of this area is still at the yield.

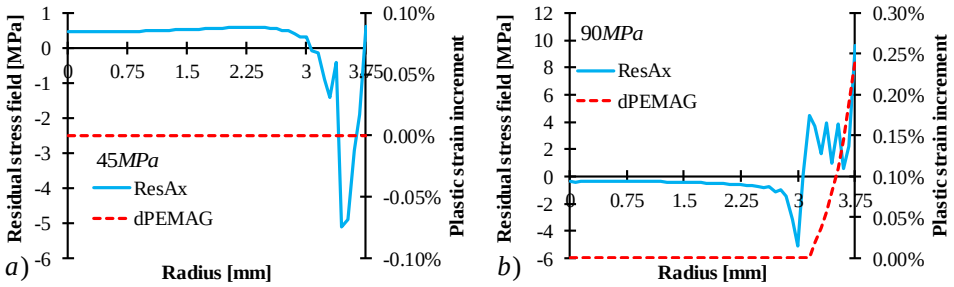

Figure 5 Axial residual stress (continuous line) and plastic strain increment (dashed line) for an applied load of a) 45 MPa and b) 90 MPa, using the EPP model and a creep dwell of 1 hour.

In order to have an increase of plastic strain (dPEMAG), the non-zero residual axial stress (ResAx) must be generated at the yielded area due to the creep stress redistribution during the creep dwell. The residual stress is calculated from the axial component of the stress, subtracting the stress field at the start of the creep dwell by the stress field at the end of it. It can be demonstrated in Figure 5 where the axial residual stress and the plastic strain increment are presented for two load cases. For a load of 45 MPa, the residual stress shown in Figure 5a is non-zero. However, for this case, the equivalent stress is not at the yield, and no plastic strain accumulates during the dwell. Conversely, for the second case, depicted in Figure 5b, both the conditions of the non-zero residual stress and yielding are satisfied and an increase of the plastic strain is observed.

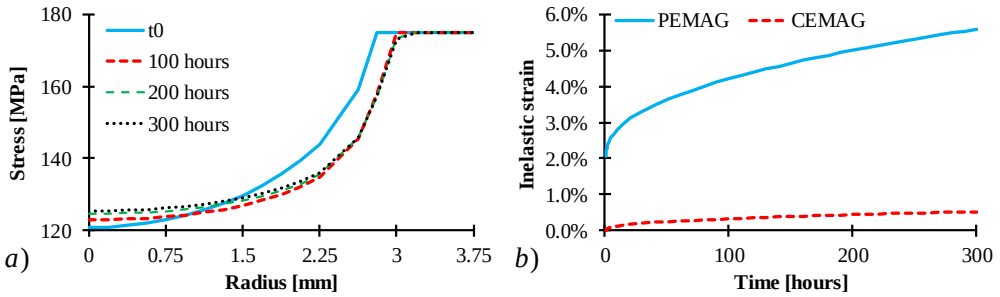

Figure 6 a) von Mises stress history with increasing dwell time using the EPP model, b) plastic and creep strain accumulation against dwell time at the notch throat.

In all the numerical cases presented so far the dwell time is equal to one hour. When a longer dwell and higher stress level are considered, the plastic strain accumulation becomes more severe. The stress along the notch throat, the plastic strain magnitude and creep strain magnitude are shown in Figure 6 for a dwell time up to 300 hours and a load of 100 MPa. When the creep dwell starts, the initial plastic strain accumulated in the most critical location is around the 2% and in less than 100 hours it is doubled. After 100 hours the increase in plastic strain is linear and reach 6% at 300 hours. The von Mises stress tends to relax progressively and to redistribute. However, at the most critical location, it is still at the yield. It is worth mentioning that the plastic strain accumulated over the 300 hours is significantly greater than the creep strain as shown in Figure 6b.

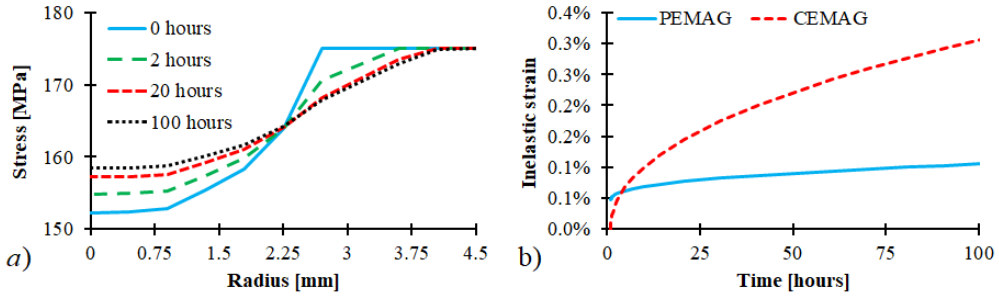

Figure 7 a) von Mises stress history along the notch throat, b) comparison between plastic strain and creep strain magnitude at the most critical location for an applied load of 150 MPa using the EPP model for a dwell time of 100 hours.

Similar results are obtained when considering the circular notched bar, but the magnitude of the plastic strain accumulation is largely reduced. As it is depicted in Figure 7a, the von Mises stress does not fully relax. After 100 hours a very small location is still at the yield, and in this area, the increment of plastic strain is observed. Despite this, the plastic strain magnitude is no larger than the creep strain magnitude (Figure 7b). In order to further verify the significance of this mechanism, a more refined plastic model has been used. The isotropic hardening model is used to model the hardening during the hot tensile testing. This is done by adopting the post-yield stress-strain response. At the load level of 90 MPa, the increase of plastic strain is not observed during the dwell. However, for a higher mechanical load of 100 MPa, the mechanism of the plastic strain accumulation caused by the high-temperature creep is demonstrated.

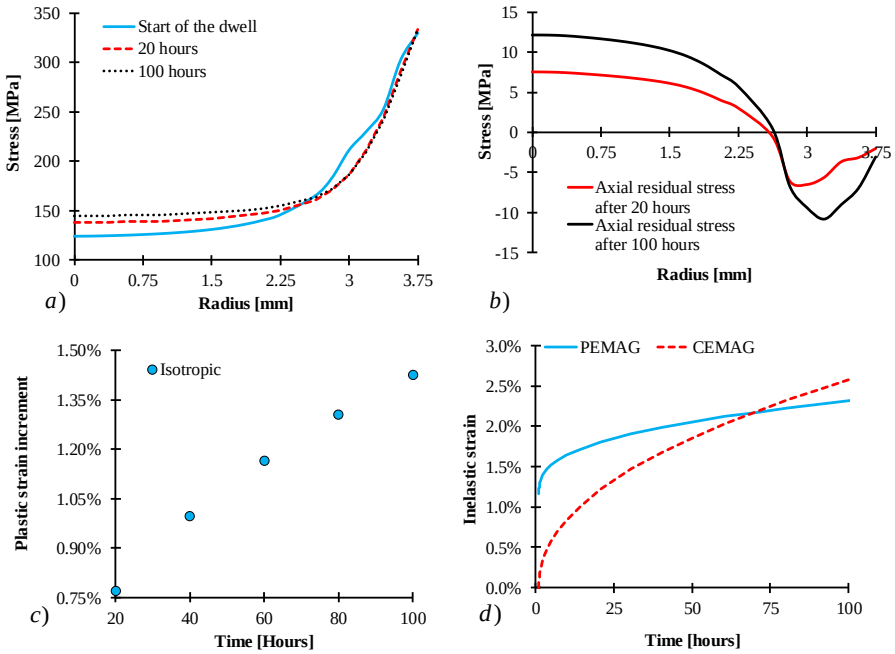

Figure 8 a) von Mises stress history along the notch throat, b) axial residual stress history, c) plastic strain increment, and d) plastic strain and creep strain magnitude at the most critical location for an applied load of 100 MPa.

The evolution of the stress is presented in Figure 8a for the most significant time points. Most of the stress redistribution occurs in the first 20 hours, affecting mostly the area between the centre of the bar up to 2.5 mm. After 20 hours an only slight increase of von Mises stress is observed in this area. Conversely, at the notch surface, the von Mises stress does not change significantly. The history of the axial residual stress is depicted in Figure 8b. The residual stress tends to increase in absolute value with the dwell time, leading to a progressive increase in the accumulated plastic strain (Figure 8c). By analysing the plastic strain increment shown in Figure 8c, a slight reduction of the accumulated plastic strain rate is observed. This is reasonable due to the use of the isotropic strain hardening, which allows a less conservative estimate of the plastic strain. Furthermore, for lower mechanical load, the plastic strain accumulation occurs only during the first few hours due to the progressive stress relaxation. A direct comparison between the plastic strain and creep strain magnitudes at the most critical location is shown in Figure 8d for an applied load of 100 MPa, where the plastic strain accumulated over the dwell is higher than the creep strain up to 75 hours. After this threshold, the creep strain magnitude becomes more significant than the plastic strain magnitude.

The mechanism of plastic strain accumulation during the high-temperature creep dwell can be described by the following mathematical statements:

$$\bar{\sigma}\left(\sigma\left(t_1\right)\right)=\sigma_y \text{ and } \bar{\sigma}\left(\sigma\left(t_2\right)\right)=\sigma_y \tag{7}$$

$$\Delta\rho_{ij}=\sigma_{ij}\left(t_2\right)-\sigma_{ij}\left(t_1\right)\Rightarrow\bar{\sigma}\left(\Delta\rho_{ij}\right)\neq 0 \tag{8}$$

Hence

$$\Delta\varepsilon^{p}\neq 0 \tag{9}$$

Where $\bar{\sigma}$ is the equivalent stress, σ_y is the yield stress, t_1 and t_2 are the time instances before and after creep dwell respectively, $\Delta\varepsilon^{p}$ is the plastic strain increment, σ_{ij} is the stress tensor and $\bar{\sigma}\left(\Delta\rho_{ij}\right)$ is the equivalent stress associated with the residual stress tensor. Eqn (2) indicates that the von Mises stress keeps unchanged at the yield during the creep dwell. However due to the creep stress redistribution, there is a non-zero residual stress ρ_{ij} as shown in Eqn (3). These two conditions inevitably lead to a plastic strain increment although there is no increase of the applied load during the creep dwell. It is important to underline that the equivalent stress will not relax, but the stress components will be affected due to the non-zero residual stress caused by the creep stress redistribution.

3.2 V-Notched bar: Cyclic Load

In this subsection, the v-notched bar is subjected to a cyclic load condition, and both the combined cyclic hardening and elastic-perfect plastic material model are used, in addition the strain hardening creep model is used instead the time hardening one. The aim of this study is to understand the possible impact of this unexpected plastic strain accumulation caused by the high temperature creep on the component's integrity. The main hypothesis is that a ratcheting mechanism can be enhanced by the additional plastic strain accumulated during the creep dwell. For both the material models considered the same cyclic loading condition is applied, an axial load range of 90 MPa with R=0. The creep dwell considered is up to 20 hours for a total of 5 full cycles for a total 100 hours. The results obtained from the EPP model are significant and are presented in Figure 9a. A progressive accumulation of the plastic strain occurs during each dwell period within each cycle. The final accumulated total plastic strain is very large, around 3.5%. However, if the more refined combined cyclic hardening model is adopted the strain accumulation is very small. This is reasonable due to the capability of the material to enlarge and move the yield surface leading to a progressive material hardening. A higher loading case of 110 MPa is further studied. The results are depicted in Figure 9 b, where the plastic strain history from the combined cyclic hardening model at 110 MPa is compared to the one from the EPP at 90 MPa. At higher loading level, even using the combined cyclic hardening material model, the plastic strain continues to increase during the creep dwell.

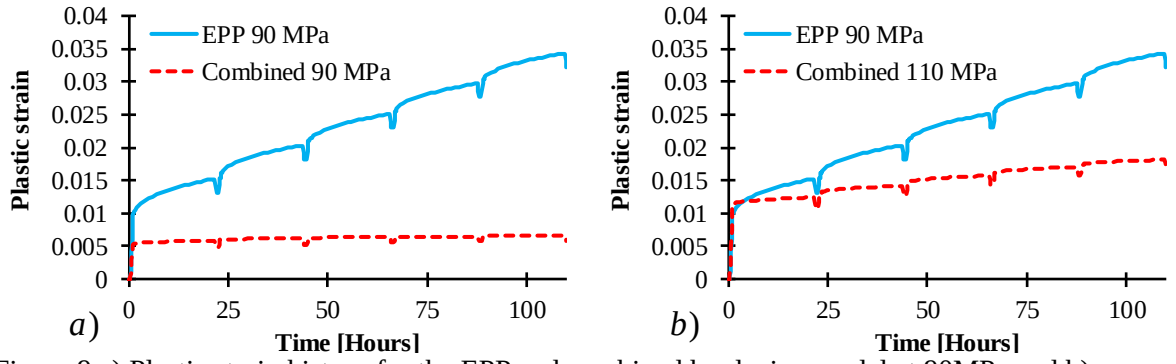

Figure 9 a) Plastic strain history for the EPP and combined hardening model at 90MPa and b) comparison between the results of EPP at 90MPa and the combined at 110 MPa.

Furthermore, for the numerical analysis that involves more than 150 full load cycles, the plastic strain accumulation does not stop as shown in Figure 10a. The plastic strain accumulation tends to saturate at around 500 hours, after which the increase is really small. This is further shown in Figure 10b, where the plastic strain history is presented for a particular load cycle during the 20 hours creep dwell. Plastic strain does not increase significantly, due to also the effect of creep response, which is different to the monotonic case seen previously.

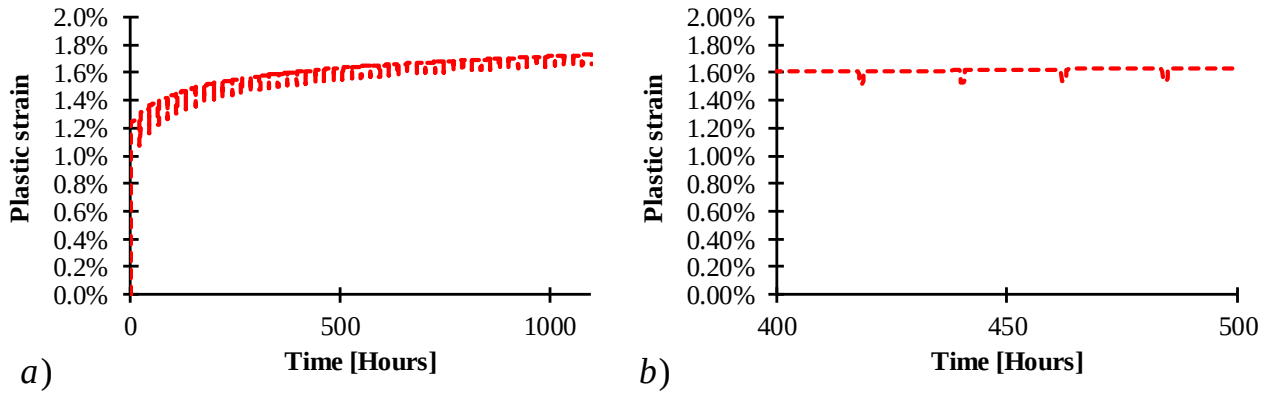

Figure 10 a) Plastic strain history for combined hardening model at 110 MPa and b) detail plot showing the plastic strain accumulation during each creep dwell.

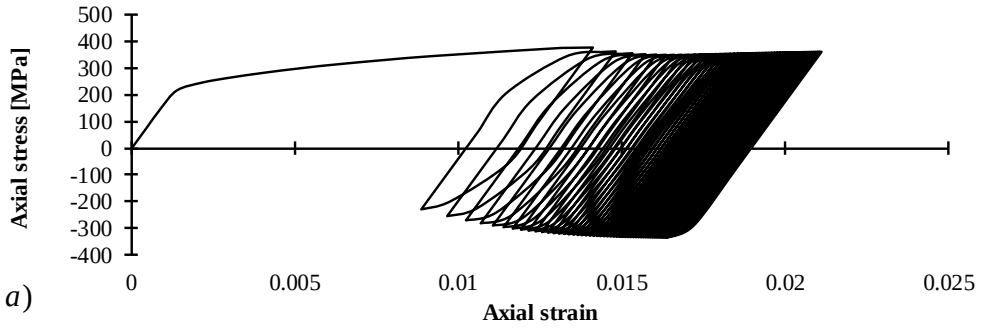

a)

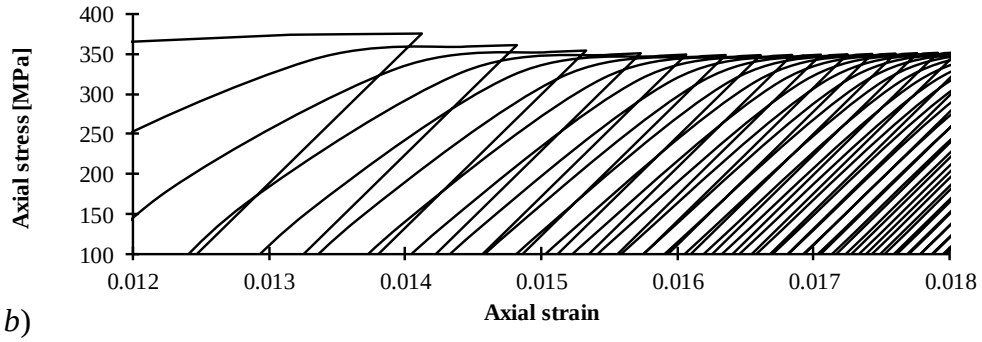

b)

Figure 11 a) Total strain history for combined hardening model and strain hardening creep model at 110 MPa and b) detail plot showing the plastic strain accumulation during each creep dwell

To have a clear picture of the cyclic response of the component the hysteresis loop is presented in Figure 11. The entire stress-strain history is showed in Figure 11a, for the axial direction. The cyclic behaviour is ratchetting but with a progressively smaller ratchet strain. The cyclic response has reached the steady state when the total axial strain is at the 1.5%. The cyclic behaviour is shown in detail in Figure 11b, since the beginning stress has a non-linear relationship with strain and a progressive peak stress relaxation can be seen. This mechanism is at the base of the progressive reduction in plastic strain accumulation. When half of the total number of cycles have been passed, the stress tends to exhibit a small further relaxation. For this cyclic load case, creep is a key contributor in halting the mechanism. In addition, this behaviour is also strongly related to the material's creep properties. For some particular structural steels, the creep properties can make the plastic accumulation process dominant even for long dwells or for less number of cycles.

This last finding further proves the importance of this mechanism, which enhances the creep-ratcheting mechanism by introducing an extra plastic strain at each load cycle. Furthermore, more extensive numerical research should be performed to investigate the impact of the creep properties.

3.3 Mesh Study

There are many sources of numerical error in a finite element analysis, one of these is the element type chosen. The potential contribution of the mesh element type and size on this unexpected but significant mechanism has been investigated by undertaking two specific studies. Both the linear and quadratic elements have been tested. In Fig 10 the effect of element type on the failure mechanism for both linear and quadratic axisymmetric elements is presented. For the V-notched bar (Fig 10a), the difference is more evident, and the quadratic element predicts a higher accumulated plastic strain during the creep dwell. Conversely, for the C-notched bar (Fig 10b), very close results are obtained with the EPP model. Also in latter case, the quadratic element predicts a higher plastic strain. The different stiffness of the element will affect only the magnitude of the phenomenon, but not its order which is always comparable. However this investigation demonstrates the same mechanism of plastic strain accumulation for all the mesh types and both notched bars.

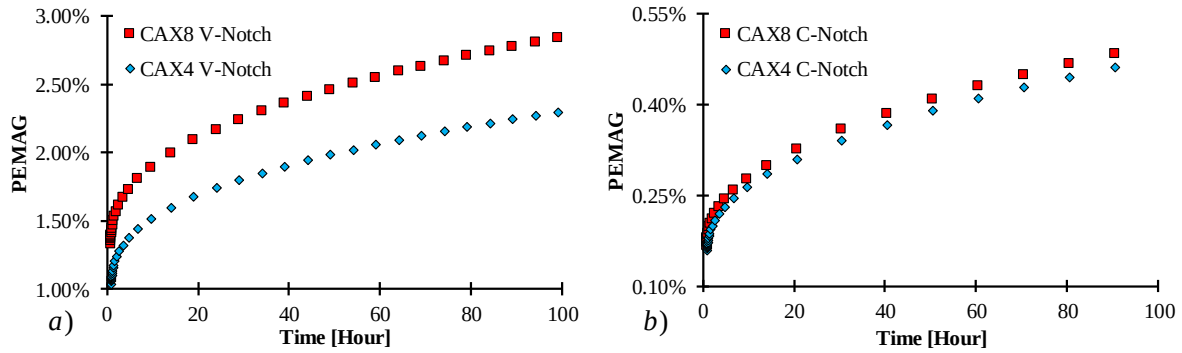

Fig 10 Effect of mesh element type on the failure mechanism for the a) v-Notched bar and b) c-Notched bar.

The second aspect investigated is the effect of the element size on the mechanism, and for this study, three meshes with an increasing number of elements have been used. The study focused on the v-notched bar using the EPP model. The element type adopted is the quadratic axisymmetric element with reduced integration scheme (CAX8). In Fig 11 the results obtained for the most critical location are reported. The mechanism is always present and affects the component despite the mesh refinement considered. The coarser mesh gives always the smallest amount of plastic strain accumulation. The results tend to converge due to the mesh refinement and a more stable value is obtained for the finer mesh. The mesh with 3660 elements predicts the same mechanism of the coarser one with 1394. However, a strong increase is observed from the coarsest mesh of 670. It is worth mentioning that any subsequent increase in the mesh density at the most critical location, does not increase the magnitude of the plastic strain accumulation.

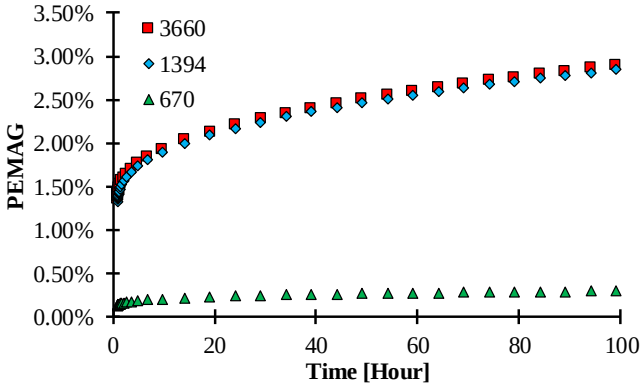

Fig 11 Effect of the mesh element size on the failure mechanism for the v-Notched bar.

4. CONCLUSIONS

A new failure mechanism of plastic strain accumulation caused by the creep stress redistribution during the high temperature dwell has been investigated and identified by an extensive use of numerical analyses. Two notched bars have been considered, a v-notched and a c-notched bar. The mechanism occurs during the high-temperature dwell when the following conditions are all satisfied for the same integration point:

i. The stress is at the yield or the yield condition is met during the dwell;
ii. A non-zero residual stress must exist and is caused by the creep stress redistribution;
iii. In order to allow the existence of a non-zero residual stress, a multi-axial stress must exist.

When this mechanism occurs, no stress relaxation has been observed in a small yielding area of the notched bar. Four major findings can be made: (i) the geometry of the notch plays a crucial role by introducing a multi-axial stress field. The v-notched bar has the highest plastic strain accumulation, meaning that this mechanism will be more severe for sharp notches. (ii) The applied load level must close to the limit load of the structure based on the EPP model. This condition has been found to be directly related to the geometry. (iii) The accuracy of the plastic model does not affect the existence of the mechanism. iv) The creep dwell is relevant for the development of the residual stress, but also for the stress redistribution process which is influenced by the creep properties. The effect of the mesh sensitivity is minimal, and only slightly affects the magnitude of the unexpected plastic strain during the dwell.

ACKNOWLEDGEMENTS

The authors gratefully acknowledge the support of the University of Glasgow and the University of Strathclyde for their support during this research.

REFERENCES

1. EDF Energy, *Assessment procedure for the high temperature response of structures, R5 Issue 3*. 2014.
2. The American Society of Mechanical Engineers, *ASME boiler & pressure vessel code : an international code, Division 1 - Subsection NH*. Vol. Division 1 - Subsection NH. 2013.
3. Isobe, N., K. Yashirodai, and K.i. Murata. *Creep Damage Assessment Considering Stress Multiaxiality for Notched Specimens of a CrMoV Steel*. in *ICMFF10*. 2015.
4. Wen, J.-F. and S.-T. Tu, *A multiaxial creep-damage model for creep crack growth considering cavity growth and microcrack interaction.* Engineering Fracture Mechanics, 2014. **123**: p. 197-210.
5. Goyal, S., K. Laha, and M.D. Mathew, *Creep Life Prediction of Modified 9Cr-1Mo Steel under Multiaxial State of Stress.* Procedia Engineering, 2014. **86**: p. 150-157.
6. Sauzay, M., et al., *Creep-fatigue behaviour of an AISI stainless steel at 550 °C.* Nuclear Engineering and Design, 2004. **232**(3): p. 219-236.
7. Dyson, B., *Use of CDM in materials modeling and component creep life prediction.* Journal of pressure vessel technology, 2000. **122**(3): p. 281-296.
8. Kachanov, L.M., *Rupture time under creep conditions.* International journal of fracture, 1999. **97**(1-4): p. 11-18.
9. Rabotnov, I.N., *Creep problems in structural members. By Yu. N. Rabotnov. Translated from the Russian by Transcripta Service Ltd., London. English translation edited by F.A. Leckie*. North-Holland series in applied mathematics and mechanics, ; v. 7. 1969, Amsterdam, London: North-Holland Pub. Co.
10. Liu, Y. and S. Murakami, *Damage Localization of Conventional Creep Damage Models and Proposition of a New Model for Creep Damage Analysis.* JSME International Journal Series A, 1998. **41**(1): p. 57-65.
11. Hyde, T.H., M. Saber, and W. Sun, *Creep crack growth data and prediction for a P91 weld at 650 °C.* International Journal of Pressure Vessels and Piping, 2010. **87**(12): p. 721-729.
12. Hyde, C.J., et al., *Application of the Liu and Murakami Damage Model for Creep Crack Growth Predictions in Power Plant Steels.* 2014.
13. Hyde, T., C. Hyde, and W. Sun, *Applied creep mechanics*. 2013: McGraw-Hill Professional.
14. Wang, W., et al., *Study of creep–fatigue behavior in a 1000 MW rotor using a unified viscoplastic constitutive model with damage.* International Journal of Damage Mechanics, 2015.
15. Holdsworth, S., *Creep-Fatigue Failure Diagnosis.* Materials, 2015. **8**(11): p. 5418.
16. Holdsworth, S.R., E. Mazza, and A. Jung. *Creep-fatigue damage development during service-cycle thermo-mechanical fatigue tests of 1CrMoV rotor steel*.
17. Barbera, D., H. Chen, and Y. Liu, *Advances on creep–fatigue damage assessment in notched components.* Fatigue & Fracture of Engineering Materials & Structures, 2017: p. 1-14.
18. Chen, H., W. Chen, and J. Ure, *A Direct Method on the Evaluation of Cyclic Steady State of Structures With Creep Effect.* Journal of Pressure Vessel Technology, 2014. **136**(6): p. 061404-061404.
19. Gorash, Y. and H. Chen, *Creep-fatigue life assessment of cruciform weldments using the linear matching method.* International Journal of Pressure Vessels and Piping, 2013. **104**(0): p. 1-13.
20. Chen, H. and A.R. Ponter, *Integrity assessment of a 3D tubeplate using the linear matching method. Part 2: Creep relaxation and reverse plasticity.* International journal of pressure vessels and piping, 2005. **82**(2): p. 95-104.
21. Chaboche, J.-L. and G. Rousselier, *On the plastic and viscoplastic constitutive equations—Part I: Rules developed with internal variable concept.* Journal of Pressure Vessel Technology, 1983. **105**(2): p. 153-158.